Facies (2010) 56:27–46
DOI 10.1007/s10347-009-0194-4

ORIGINAL ARTICLE

Meteoric diagenesis of Quaternary carbonate-rocky talus slope successions (Northern Calcareous Alps, Austria)

Diethard G. Sanders · Marc Ostermann · Jan Kramers

Received: 14 January 2009 / Accepted: 20 July 2009 / Published online: 12 August 2009

Abstract In the Northern Calcareous Alps (NCA), meteoric cementation of Quaternary talus slopes was mainly sourced by dissolution of matrix and lithoclasts, by leaching of glacial till, and by groundwaters entered from underneath. Cement precipitation can take place within a few hundreds to a few thousands of years after talus deposition, but later diagenetic changes locally are indicated. Downslope along well-preserved talus successions, a change in prevalent diagenetic pathways is related to prolonged availability of pore waters from the apex to the toe of the slope. Talus slopes contain a significant proportion of carbonate mud probably produced by a combination of physical, chemical, and biological processes. $^{234}U/^{230}Th$ cementation ages of talus successions are scattered over a total range of 5–480 ka. The talus relicts of the NCA thus became cemented at highly different times during the late Quaternary. With the available data, we could not identify a specific palaeoclimatic significance of talus cementation.

Keywords Eastern Alps · Quaternary · Talus slopes · Diagenesis · Cementation · Uranium–thorium

Introduction

In the Northern Calcareous Alps (NCA), erosional relicts of lithified Quaternary talus-slope successions are common (Fig. 1). A talus slope is defined as an accumulation of "Rock fragments of any size or shape (usually coarse and angular) derived from and lying at the base of a cliff or very steep, rocky slope" (Bates and Jackson 1980, p. 638). Talus slopes are distinct depositional systems that form only in ensemble with degrading rock cliffs. In the present Eastern Alps, post-glacial talus successions up to more than 100 m in thickness are widespread (Schrott et al. 2004).

In a previous paper, based on observations both in lithified talus relicts and on active talus slopes, the facies and facies architecture of mature talus-slope successions have been described (Sanders et al. 2009). For the NCA, by analogy to a well-preserved, lithified talus-to-alluvial fan succession of Eemian age (Ampferer 1914; Sanders and Ostermann 2006), a long-traded working hypothesis was that lithified talus relicts formed during the Riss–Würm interglacial. $^{234}U/^{230}Th$ age-dating of cements of talus relicts proved this hypothesis obsolete (Ostermann 2006).

In the present paper, the diagenetic patterns and results of U/Th age-dating of cements in the talus relicts are described. Typical diagenetic pathways can be placed into a concept of talus-slope development in space and time. Our observations reveal an unexpectedly high content of talus-slope successions in carbonate mud. Aside of karstic dissolution and production of coarse rock fragments, carbonate-rocky mountains such as the NCA thus initially degrade under production of a substantial amount of micrite.

Electronic supplementary material The online version of this article (doi:10.1007/s10347-009-0194-4) contains supplementary material, which is available to authorized users.

D. G. Sanders (✉) · M. Ostermann
Institute of Geology and Palaeontology,
University of Innsbruck, Innrain 52,
6020 Innsbruck, Austria
e-mail: Diethard.G.Sanders@uibk.ac.at

J. Kramers
Institute of Geological Sciences,
University of Berne, 3012 Bern, Switzerland

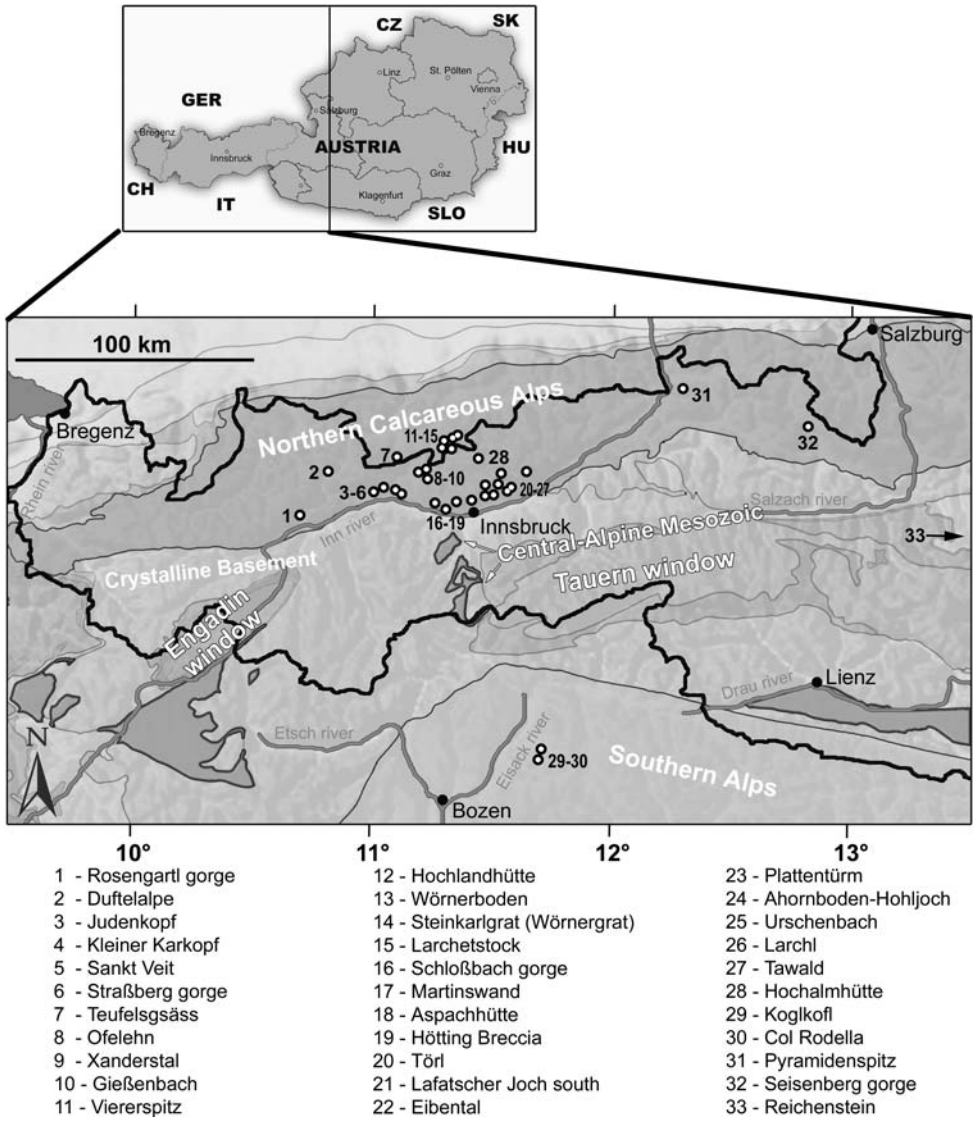

Fig. 1 Overview of the western part of the eastern Alps, and position of investigated lithified talus successions. The Northern Calcareous Alps (NCA) comprises a stack of cover thrust nappes dominated by Triassic carbonate rocks (see Fig. 2). The Central-Alpine Mesozoic consists mainly of two thick successions of metadolostones

Geological frame

The NCA comprise a package of cover thrust nappes derived from the former northern margin of the Apulian plate (Austroalpine tectonic units) (Schmid et al. 2004). The NCA are dominated by two thick successions of Triassic platform carbonates, each underlain by a thinner unit with sulfate evaporites (Fig. 2). The sulfate evaporites served as main decollement horizons during Alpine orogenesis. Most of the cliffs and summits of the NCA consist of platform carbonates of the Wetterstein Limestone or of the Hauptdolomit–Dachstein Limestone unit (see Fig. 2); these stratigraphic units produce most of the morphological relief for the formation of talus slopes. For talus lithification, the incompetent sulfate-bearing units sandwiched along overthrusts also are significant because they favor the formation of groundwaters supersaturated for calcium carbonate (Sanders et al. 2008; Sanders and Wertl 2009). On terrains of non-metamorphic dolostones (Hauptdolomit unit, Fig. 2), talus lithified by calcitic cements is extremely rare and confined to patches a few meters in size. On the metadolostone terrains of the Central-Alpine Mesozoic (Fig. 1), no lithified talus relict was found.

The carbonate-lithic talus slopes of the NCA developed in a specific fashion: after deglacial exposure of rock cliffs, a rock glacier or a low-dipping immature talus slope dominated by unsorted rockfalls accumulated at first (Fig. 3). With progressive buildup and onlap of a talus slope onto the retreating rock cliff, a differentiation of the slope into segments of different dip develops. Concomitantly, prevalent processes change to grain flows and 'sorted' rockfall deposition in the proximal, steep-dipping (35–30°) slope segment while deposits of cohesive debris-flows, ephemeral fluid flows and large rockfalls prevail in the distal, lower-dipping slope segment. The proximal slope segment is separated from the distal segment by a distinct knick in

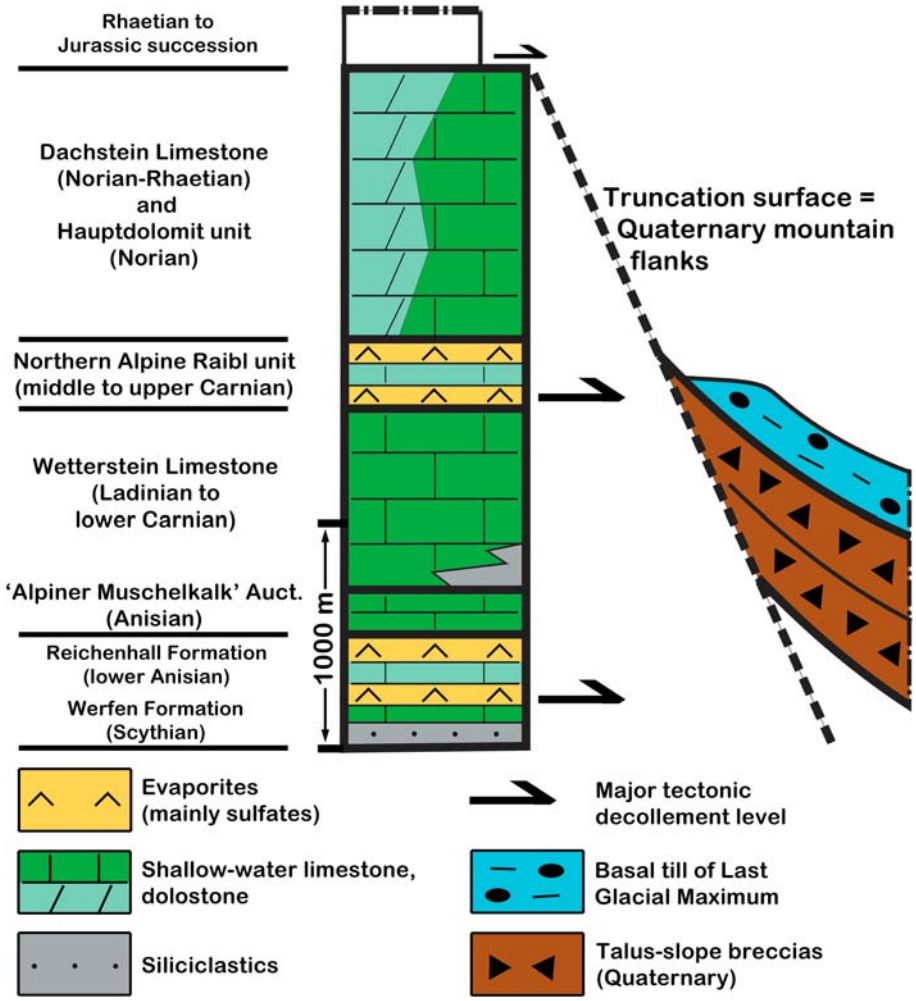

Fig. 2 The Triassic succession of the NCA is dominated by two thick packages of platform carbonates, the Wetterstein Limestone, and the Dachstein Limestone and its lateral equivalent, the Hauptdolomit unit. Stacking of cover thrust nappes took place mainly along decollement levels with sulfate evaporites. In the NCA, rocks of Rhaetian to Jurassic age comprise a comparatively thin succession that is of minor significance with respect to landscape development

slope. In mature talus deposystems, the aggrading–prograding proximal slope succession thus sheds over the lower-dipping package of the distal slope along a thin 'downlap interval'. Finally, talus accumulation strongly diminishes; in this late stage, many talus slopes become subject to localized linear erosion and development of secondary alluvial fans (Fig. 3). The sedimentary facies of the talus successions are characterized in Table 1 (see Sanders et al. 2009, for more detailed description).

There is no sharp separation between unlithified and lithified talus successions, respectively. For instance, talus slopes accumulated after the Last Glacial Maximum (LGM, 21–18 ka, Patzelt 1980; Van Husen 1999) often are cemented along discrete layers (Fig. 4a). The term 'partly lithified talus' herein is used for successions cemented along discrete layers or in patches only. The investigated lithified talus relicts are preserved either uncovered, or are overlain by glacial till of the LGM, and/or by vegetated soil (Fig. 4b). In partly lithified, post-glacial talus deposits, the products and pathways of diagenesis are basically identical to those of older talus relicts.

Methods

A total of 33 lithified or partly lithified talus successions were investigated (Fig. 1). Cut and polished rock slabs and 122 thin sections provided documentation of textures and diagenesis. Stable isotopes of oxygen and carbon were measured of lithoclasts, matrices, and cements. For isotope measurements, cleaned and polished rock slabs were excavated with a dental drill (Ø 0.3–1 mm). Isotope samples were measured on a Finnigan DeltaPlusXL mass spectrometer connected with a gas bench (see Spötl and Vennemann 2003, for Method). Polished thin sections were investigated under cold cathodoluminescence (Technosyn 8200 MK II) and epifluorescence (Nikon Eclipse E400POL). For comparison, active unlithified talus slopes were investigated for their content in fine-grained matrix. Analyses of stable isotopes values of oxygen and carbon from the matrix and from the lithoclasts of active talus slopes were done to better understand the origins of fine-grained matrix in the lithified talus relicts (see Electronic supplementary material for details).

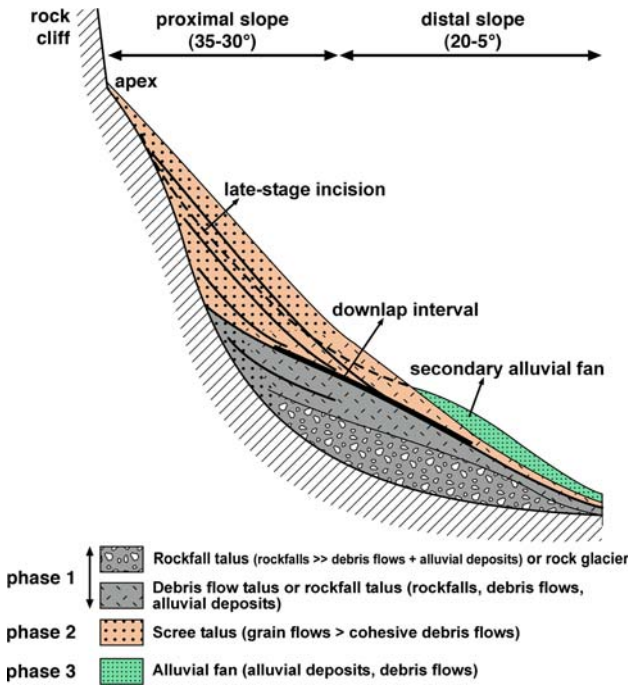

Fig. 3 Generalized scheme of talus-slope development. *Phase 1* (slope-front filling): subsequent to deglaciation at site, a rock glacier or a low-dipping talus dominated by rockfalls and by cohesive debris flows develops. *Phase 2* (climbing onlap and progradation of talus slope): the onlap of the talus slope climbs up along the toe of the retreating rock cliff. Concomitantly, the slope lengthens and steepens to 30–35°, and grain flows become prevalent. During this phase, the talus slope sheds over and downlaps onto the underlying slope-front fill along a thin 'downlap interval'. *Phase 3* lengthening of slope combined with declining sediment input from the retreating/lowering rock cliff progressively slows accumulation. In this late stage, many talus slopes become subject to linear erosion, and secondary alluvial fans may develop

For $^{234}U/^{230}Th$ dating of cements, fringes of calcite orthosparite were sampled with a microdrill under the microscope. After physical removal of organic material, the samples were chemically prepared for uranium and thorium, spiked with a $^{236}U + ^{229}Th$ spike. U and Th measurements were done in a Nu-Instruments MC-ICP mass spectrometer. To correct for detrital contamination, the main problem in age-dating authigenic carbonates (Kaufman 1993; Debaene 2003), we chose the regression line method based on at least three sub-samples (cf. Ludwig and Titterington 1994; Lin et al. 1996; Frank et al. 2000; Geyh 2001, 2005; Mallick and Frank 2002) plotted in $^{230}Th/^{232}Th$ vs. $^{234}U/^{232}Th$ activity diagrams (Rosholt 1976) ("Rosholt diagrams"). Age calculation was done by a Th–U disequilibrium age calculation program (Visual Basic, written by Jan Kramers, according to the equation of Kaufman and Broecker 1965). The errors of calculated ages are indicated as 2 sigma standard deviation (see Ostermann et al. 2006a, 2007, for detailed description of method). We tested the

Table 1 Prevalent facies of lithified carbonate-rocky talus slopes (Northern Calcareous Alps), and their characteristic features of diagenesis

Facies	Characterization	Typical position	Features of diagenesis
Rockfall breccias	Typically unbedded, extremely poorly to very poorly sorted, clasts angular, isotropic clast fabric, no primary matrix	Thicker intervals: in basal and distal part of talus successions. Rarely preserved	Micritic cement, pockets with infiltrated secondary matrix
Grain flow breccias	Well-stratified, poorly to well-sorted fine gravel to cobbles, clasts angular–subangular, no primary matrix	Proximal part of mature talus slopes	Micritic cement fringes, fringes of skalenohedral calcite cement, infiltrated secondary matrix
Breccias to conglobreccias of matrix-bearing (cohesive) debris flows	Very poorly to extremely poorly sorted, indistinctly bedded, clast- to matrix-supported, primary matrix of lime mudstone to silty-sandy lime mudstone	Proximal to distal part of talus slopes	Lithification of lime mud, development of secondary porosity by eluviation and/or dissolution of matrix
Breccias to conglobreccias deposited from fluid flows	1. Channel fills: lenses of extremely poorly sorted fine gravels to boulders, clast openwork or matrix of winnowed sand 2. Sheet-flow deposits: distinctly subparallel stratified, well-sorted openwork gravel to sand, arranged in stacked gravel/sand rhythms	Distal part of talus slopes	Channel-fills: micritic cement, pockets with infiltrated secondary matrix Sheet flow deposits: Micritic cement, fringes of skalenohedral calcite cement, levels with infiltrated secondary matrix (that may fill entire interstitial pore space)

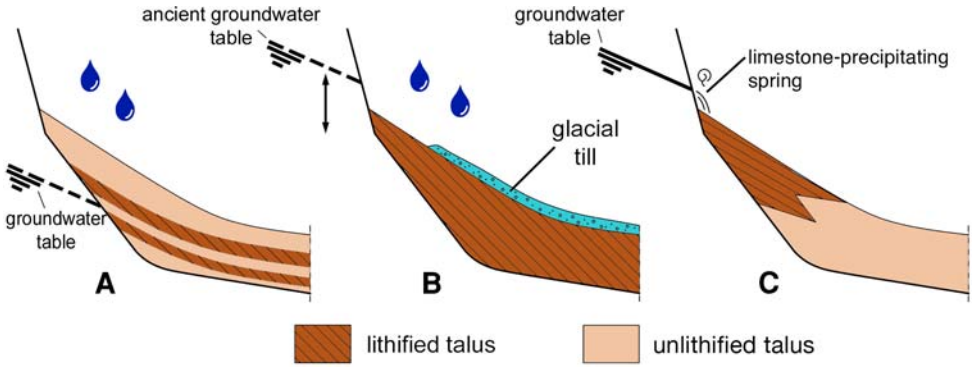

Fig. 4 Lithification of talus slopes. **a** Stratabound lithification of talus slopes accumulated after the last glacial maximum (*LGM*). This style of lithification is limited to cementation of openwork clast layers. **b** Full lithification, as common in pre-LGM talus relicts. **c** Talus slopes cemented in association with limestone-precipitating spring (see also Fig. 5)

validity of the U/Th method in talus slopes and alluvial fans for which a post-glacial age is firmly established by chronostratigraphy and/or by other radiometric methods (Ostermann 2006; Ostermann et al. 2006b). In all these cases, post-glacial ages of cementation resulted; this underscores that age-dating of cements by the U/Th method can provide geologically meaningful results. In most other cases, however, we chose the cements of lithified talus relicts of unknown age. In the following, settings of talus lithification and U/Th ages of cements are characterized.

Settings of talus lithification

Stratabound cementation

In talus successions of late-glacial to post-glacial age, individual beds or bedsets with openwork clast fabric may be lithified by micritic cement and/or by fringes and pendants of calcite orthospar cement (Fig. 4a). Overall, down-section within these successions, the abundance and thickness in particular of calcite spar cements tends to increase. In the partly lithified talus successions, matrices of carbonate mud to silt are firm but friable. Except for talus slopes associated with limestone-precipitating springs (see below), in none of the partly cemented successions lithification within the topmost few meters was observed.

Complete lithification

Many of the fully lithified talus relicts of the NCA are overlain by basal till of the LGM (Fig. 4b), which provided a criterion on their minimum age (cf. Ampferer 1907, 1935). These talus relicts comprise lithified lime–muddy matrices and diverse types of calcitic spar cement. In lithified talus relicts that are well preserved from apex to toe, an overall downslope trend in diagenetic products is recognized (see farther below). In all cases, openwork clast fabrics tend to contain the best-developed fringes of calcite spar cement; this is relevant for U/Th dating.

Limestone-spring setting

A few limestone-depositing spring deposystems of the Eastern Alps are associated with lithified talus slopes (Figs. 4c and 5) (Sanders et al. 2006a, 2006b). Talus slopes downstream of limestone-precipitating springs typically are lithified in their apical to proximal part; farther downslope, stratabound cementation may occur. Except for an overall scarcity of geopetally infiltrated matrices of lime mud, the diagenesis of these talus slopes shows all the features also observed in lithified talus successions not associated with limestone springs.

Ages of cementation

Our U/Th cementation ages of selected talus relicts indicate that lithification took place time and again during the Quaternary, over a total documented age range from 5 to 480 ka (Table 2). The latter represents the oldest cementation age so far identified for a talus relict in the Eastern Alps. The long-traded hypothesis that most, if not all, lithified talus relicts of the NCA accumulated and lithified during the Eemian thus is obsolete (Ostermann 2006). The age data, however, are too few to identify potential phases of enhanced talus cementation.

Within the resolution of microdrill sampling, we found no evidence for separate phases of precipitation of petrographically early spar cement; potentially discrete phases of cement formation thus may be contained with the 2 sigma standard error of age resolution (Ostermann et al. 2006b). U/Th dating of calcite cements from talus successions that, by their physical stratigraphic relations, clearly are of late-glacial to post-glacial age in all cases yielded ages consistent with their stratigraphic position. This provided a simple, additional check of correctness of the calculated numerical cementation ages from pre-LGM talus successions. The dated cements from the post-glacial talus successions indicate that lithification (including fringes of sparitic cement) can start a few hundreds to a few thousands of years after accumulation of a talus slope (Ostermann 2006).

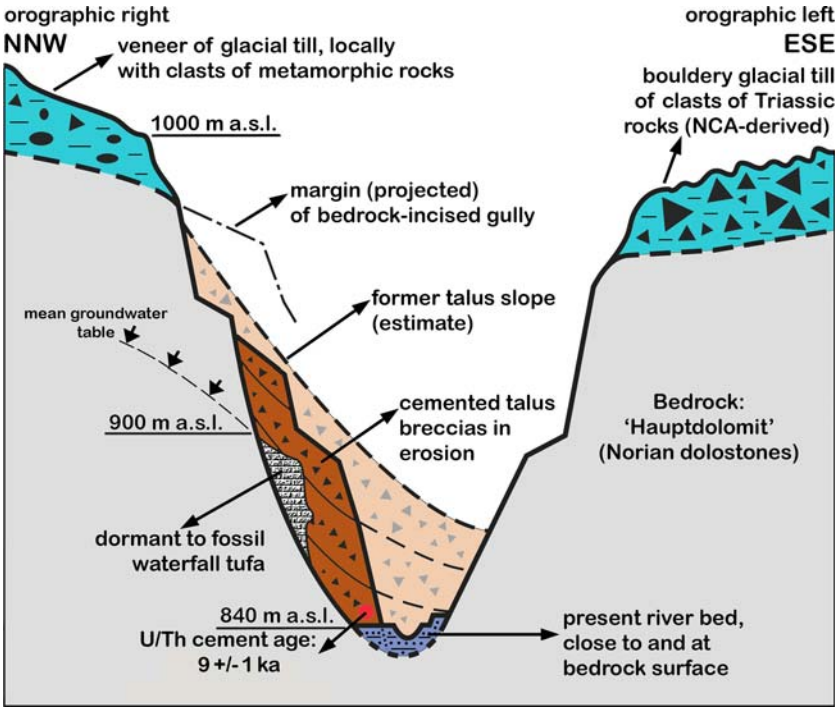

Fig. 5 Talus cementation associated with limestone spring, Straßberg gorge, Mieming massif. Section across the gorge showing talus slopes subject to cementation by limestone-precipitating springs that emerge at 900 m a.s.l. Today, the cemented talus slopes are largely undergoing erosion, but localized cementation is still taking place. The gorge is incised into a glacially formed valley that is veneered by glacial tills. U/Th dating of cement of a sample of talus breccia yielded an Early Holocene age (see Table 2)

Diagenetic products

Lithified lime mud (primary and secondary matrices)

Petrographically, the diagenesis of matrices of lime mud is merely reflected in lithification (Fig. 6a, b). Aside of primary matrices of lime mudstone to carbonate-lithic wackestone devoid of depositional structures, geopetally laminated secondary matrices of lime mudstone are widespread. Secondary matrices are typical within openwork fabrics of gravels to cobbles that, for instance, accumulated from grain flows or from ephemeral fluid flows. Geopetally infilled secondary matrices are common both in non-lithified post-glacial talus (Fig. 6c, d) and in fully lithified older talus relicts (Fig. 6e, g). In many cases, the pore space is completely filled by secondary matrices.

Secondary porosity

Herein we use the term secondary porosity to designate all 'generations' (secondary, tertiary, etc.) of pores developed subsequent to primary porosity. In lithified talus, (a) remnant interstitial pores in cemented openwork clast fabrics, and (b) pores from vadose eluviation and/or dissolution of matrix are widespread. In a debris-flow layer of a post-glacial talus excavated for a civic well, along the contact between lithoclasts and fine-grained matrix, the matrix is riddled by a dendritic network of hollow veins (Fig. 6h). Up-section, the veins gradually taper out by thinning. Down-section, the veins debouch into the pore space of a layer of openwork breccia. Along the base of the openwork breccia, a layer of geopetally laminated, firm lime mud is present. This layer, in turn, is riddled by a vein network. A few of the veins are clad with a thin fringe of indurated micrite, although the surrounding matrix is unlithified (Fig. 7a). At the same location, along discordant pathways of preferred down-slope percolation of vadose water, the primary matrix has been swept out from the interstitial pore space. The resulting fabric is that of a subvertical dyke up to a few decimeters in width of clast-supported openwork breccia that is embedded within host breccia with lime–muddy matrix (Fig. 7b). Clear water splashed out of such a dyke with a rate of a few liters per second. Discordant dykes of clast-supported openwork breccia lithified by calcite cement have been observed in fossil, lithified successions of alluvial fans and talus slopes.

In lithified talus relicts, both primary and secondary matrix may be riddled by micro- to mega-pores fringed by calcite cement (Figs. 6f, 7c, d, e). In many cases, the matrix infills are truncated along erosional surfaces which, in turn, are overlain by another generation of secondary matrix (Fig. 7f). Depending on the host rocks that fed a talus slope, lithomouldic pores may be present. Lithologies that commonly undergo partial or wholesale dissolution are cellular dolostones and marly dolostones. The lithomoulds may be partly or entirely filled by geopetally laminated lime mudstone, and/or may be fringed by cements. Many lithoclasts became dissolved from their margin or their center outward.

Table 2 $^{234}U/^{230}Th$ disequilibrium ages of cements in talus successions, Northern Calcareous Alps, arranged in order of increasing age (Ostermann 2006)

Location	Type of talus Degree of lithification	U/Th age of cement Setting of lithification
Rosengartl gorge (location #1 in Fig. 1)	Rockfall talus	8.3 ± 0.6 ka
	Partly lithified	Seepage setting
Urschenbach (location #25 in Fig. 1)	Debris flow talus	8.6 ± 0.6 ka
	Partly lithified	Talus slope setting
Straßberg gorge (location #6 in Fig. 1)	Scree talus	9 ± 1 ka
	Partly lithified	Spring-limestone setting
Schloßbach gorge (location #16 in Fig. 1)	Scree talus	9.6 ± 0.6 ka
	Partly lithified	Seepage setting
Larchl (Hinterhorn) (location #26 in Fig. 1)	Scree talus	45.3 ± 1.7 ka (range: 30–60 ka)
	Lithified	Talus slope setting
Hohljoch (Ahornboden) (location #24 in Fig. 1)	Alluvial talus	68 ± 3 ka
	Lithified	Talus slope setting
Hötting Breccia (location #19 in Fig. 1)	Scree talus	109 ± 6.5 ka
	Lithified	Talus slope setting
Col Rodella (location #30 in Fig. 1)	Debris flow talus	116.5 ± 7 ka
	Lithified	Talus slope setting
Judenkopf (location #3 in Fig. 1)	Scree talus	122 ± 7.7 ka
	Lithified	Talus slope setting
Törl (location #20 in Fig. 1)	Scree talus	181 ± 20 ka
	Lithified	Talus slope setting
Teufelsgsäss (location #7 in Fig. 1)	Debris flow talus	480 ± 20 ka
	Lithified	Talus slope setting

See Fig. 1 and electronic supplementary material for position and details of locations. Error ranges of ages refer to the 2 sigma standard deviation (see electronic supplementary material for Rosholt diagrams)

Less commonly, the surface of lithoclasts shows an embayed, pitted outline while the inner part of the clasts is intact (Figs. 6e, 7g).

Cements

Micritic cements

In openwork clast fabrics and in secondary pores, crusts of isopachous to mammillary to pendant shape of micritic cement are widespread (Figs. 7h and 8a, b, c). In a few samples, micritic crusts interlaminated with orthosparitic calcite cement are present. Another uncommon type of micritic cement is represented by crusts up to about 10 mm thick of clotted lime mudstone; the mudstone displays a 'wrinkly' lamination subparallel to clast surfaces (Fig. 7h).

Isopachous fringes of calcite orthospar

Fringes of skalenohedral calcite cement are widespread (Fig. 8a, b, c, d. e), and are well suited for U/Th age-dating. In cathodoluminescence, all investigated calcite spar cements were non-luminescent. The cements typically overlie a crust of micritic cement directly on the clasts, and most commonly to do not completely fill the pore space. In partly lithified, post-glacial talus successions, the openwork layers are mainly lithified by fringes of calcite cement (Fig. 7a); in the lower part of the openwork layers, the interstitial pore space may be clogged by geopetally laminated carbonate silt to mud that is firm, but friable (Figs. 6c, d, 8f).

Meniscus cement, 'water-level cements'

Meniscus cements formed within the adhesive meniscus of water at clast contacts are common. The water-level cements, by contrast, are geopetally oriented and precipitated along free, vadose water levels within wider megapores (Fig. 8a, b, c, g). Water-level cements are typically present in stacks of up to more than ten levels (Fig. 8g).

Microstalactites

In openwork fabrics of gravels to cobbles, microstalactites up to 1.5 cm in length of calcite cement are locally present

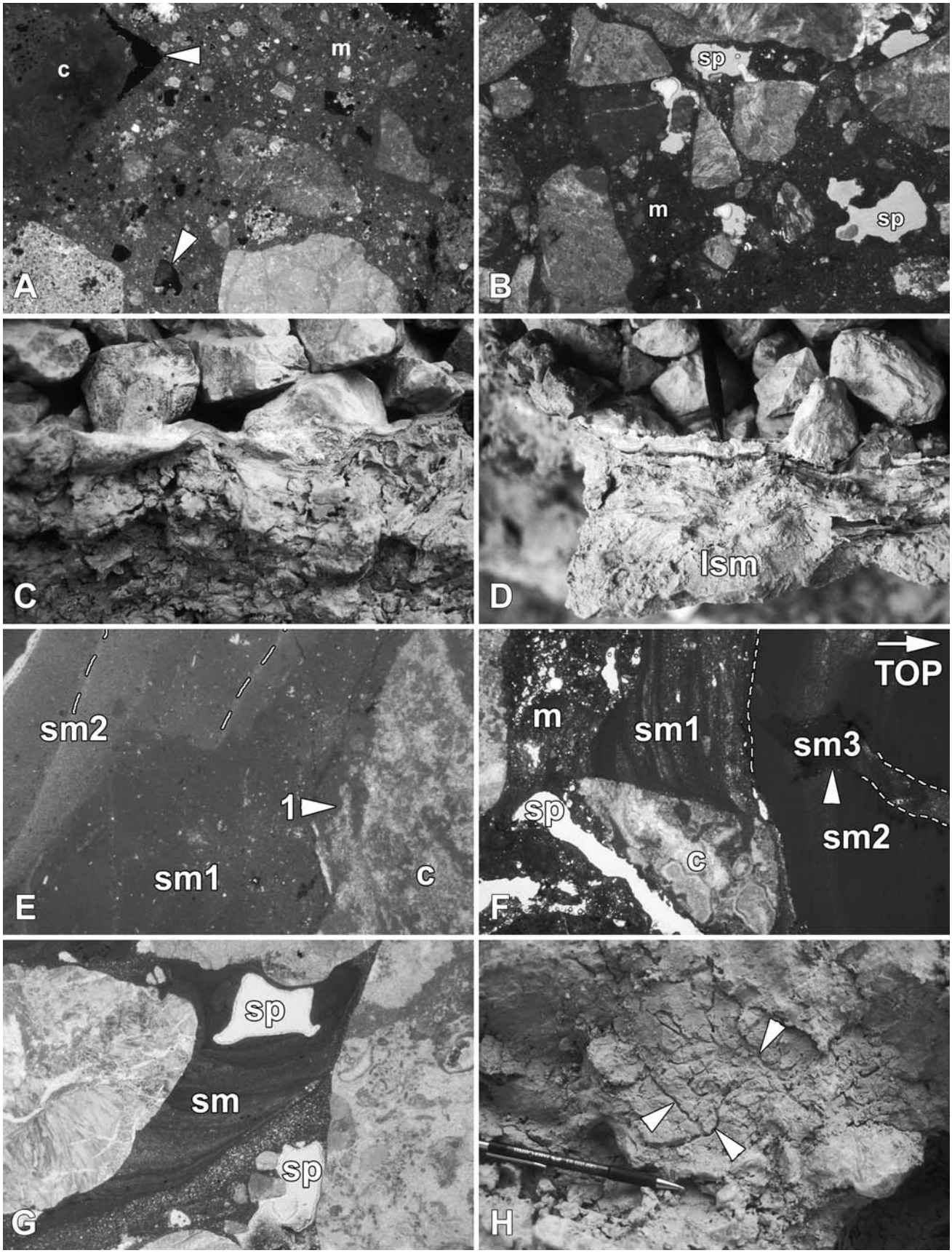
c
m
A
sp
m
sp
B
C
lsm
D
sm2
1
sm1
c
E
m
sm1
TOP
sm3
sp
sm2
c
F
sp
sm
sp
G
H

◀ **Fig. 6** Diagenetic features of lithified talus, Northern Calcareous Alps. **a** Breccia deposited from cohesive debris flow with a primary matrix (*m*) of carbonate-lithic wackestone to packstone. An angular shape of some of the open pores (*black patches*, some labelled by *arrowtips*), in part along the edges of lithoclasts (*c*) suggests that they represent lithomouldic pores. Xanderstal, Ahrnspitz group. Crossed nicols. Width of view 17 mm. **b** Breccia deposited from cohesive debris flow with a primary matrix (*m*) of carbonate-lithic wackestone. Note open secondary pores (*sp*). Tawalder Reissn, Karwendel. Width of view 17 mm. **c** Detail of open well pit in post-glacial talus slope. The *upper part* of the photo shows the lower part of a cemented layer of openwork breccia. In the *lower part* of the photo, the interstitial pore space is filled by geopetally laminated secondary matrix of lime mud. Sankt Veit, Mieming massif. Width of view 22 cm. **d** Detail of **c**, showing geopetal lamination of secondary matrix (*lsm*). Width of view about 21 cm. **e** Detail of talus breccia deposited from ephemeral surface runoff. In the *right part* of the photo, a carbonate lithoclast (*c*) is visible. Note pitted and embayed outline (*arrowtip 1*) of clast. The central and left portion of photo shows a secondary matrix (*sm1*) of carbonate-lithic wackestone to lime mudstone. Within secondary matrix *sm1*, in turn, a surface of irregular, differentiated shape (*dashed lines*) is overlain by another 'generation' of secondary matrix (*sm2*), of laminated lime-mudstone. Xanderstal, Ahrnspitz massif. Width of view 17 mm. **f** Detail of talus breccia deposited from ephemeral surface runoff. Besides of lithoclast (*c*), note relicts of a primary matrix (*m*), overlain by geopetally laminated secondary matrix *sm1* of lime mudstone. Secondary matrix *sm1* is overlain by secondary matrix *sm2* of lime mudstone. Within secondary matrix *sm2*, a discordant vein (partly highlighted by *dashed line*) is present which, in turn, became filled by secondary matrix *sm3*. Note also the presence of open secondary pores (*sp*). Hohljoch-Ahornboden breccia, Karwendel. Width of view 17 mm. **g** Thin section of torrential conglobreccia. The interstitial pore space is filled by geopetally laminated secondary matrix (*sm*) of lime mudstone to calcisiltite. A network of open secondary pores (*sp*) became fringed by very thin crusts of calcite cement. Hötting Breccia, Karwendel. Width of view 17 mm. **h** Open well pit in post-glacial talus slope. Cohesive debris flow deposits above the openwork layer shown in **c**, about 4.3 m below present surface. Photo shows matrix of lime mud to calcisiltite along the negative print of the surface of a cobble-sized lithoclast. In the matrix along the former clast surface, a dendritic network of open veins (a few labelled by *arrowtips*) about 1–5 mm in width is present. Sankt Veit, Mieming massif. *Pen* is 14.5 cm in length

(Fig. 8f, g, h). The microstalactites typically consist of short calcite 'tubes' that are open at their lower (drip) end, but that are more densely calcified in the upper, proximal part of the stalactites (Fig. 8f, g, h). Internally, the microstalactites consist of porous fabrics of skalenohedral calcite crystals that radiate inward from the surface of the microstalactites.

Stable isotope values of oxygen and carbon

The stable isotope values of oxygen and carbon of talus breccias overall show a roughly co-variant decrease from most positive values of $\delta^{18}O$ and $\delta^{13}C$ of the lithoclasts ('host rocks') towards more negative values for fine-grained matrices and, finally, to most negative values of sparitic calcite cements. This trend holds both for the sum of measured values from all investigated locations (Fig. 9), as well as—with much variation—for individual locations.

Interpretation

Diagenetic fabrics

The lithification of lime–muddy matrices proceeded by dissolution–reprecipitation on a scale of microns. This is supported by the position of the stable isotope values of matrices intermediate between host rocks and orthosparitic cements (Fig. 9). The secondary pores in the matrices probably are of multiple origins: The described dendritic network of open veins in the matrix, combined with presence of cement in the downward-adjacent openwork layer indicate that both eluviation and dissolution of matrix take place in that case. In fully lithified talus relicts, secondary pores along the surface of lithoclasts are common; this suggests that such vein networks are widespread. From an unlithified, high-alpine talus cone, small fenestral pores interpreted as products of ice segregation are described; such pores may need at least 30–50 freeze/thaw cycles to form (Bertran and Texier 1994). Porosity from ice segregation might attain 25–30% of total matrix volume, resulting in a fabric herein dubbed 'pseudo-loferitic' (cf. Van Vliet-Lanoe 1976; Bertran and Texier 1994). Our thin sections of lithified talus relicts suggest that ice-segregation pores might indeed comprise a part of secondary porosity, but we did not observe pseudo-loferitic fabrics.

The mentioned truncation surfaces within the matrices indicate periods of (a) intense pore-water flow and eluviation and/or (b) localized dissolution of matrix. In many cases, the phases of internal erosion were followed by another infilling of secondary matrix. For a few talus successions, a common presence of lithomoulds suggests that dissolution of diagenetically unstable lithoclasts may represent a significant source of dissolved calcium carbonate for cementation. Because of their typical position directly at the surface of lithoclasts, the micritic cements formed first, most probably in a vadose diagenetic environment. Conversely, the isopachous fringes of skalenohedral calcite formed in an essentially phreatic diagenetic environment, typically deeper within the succession.

Stable isotopes

The covariant trend towards more negative values of both $\delta^{18}O$ and $\delta^{13}C$ from lithoclasts via matrices to sparitic cements (Fig. 9) indicates diagenesis in meteoric waters (Hoefs 1997; Lohmann 1988). With respect to the figures of stable isotope values and the relative isotope shift from clasts to cement, however, we could not identify a single pattern. The $\delta^{13}C$ and $\delta^{18}O$ values of the matrices plot closer to the values of lithoclasts than the corresponding sparitic cements. The isotope values of matrices thus probably are rock-buffered to some degree. The $\delta^{13}C$ of meteoric

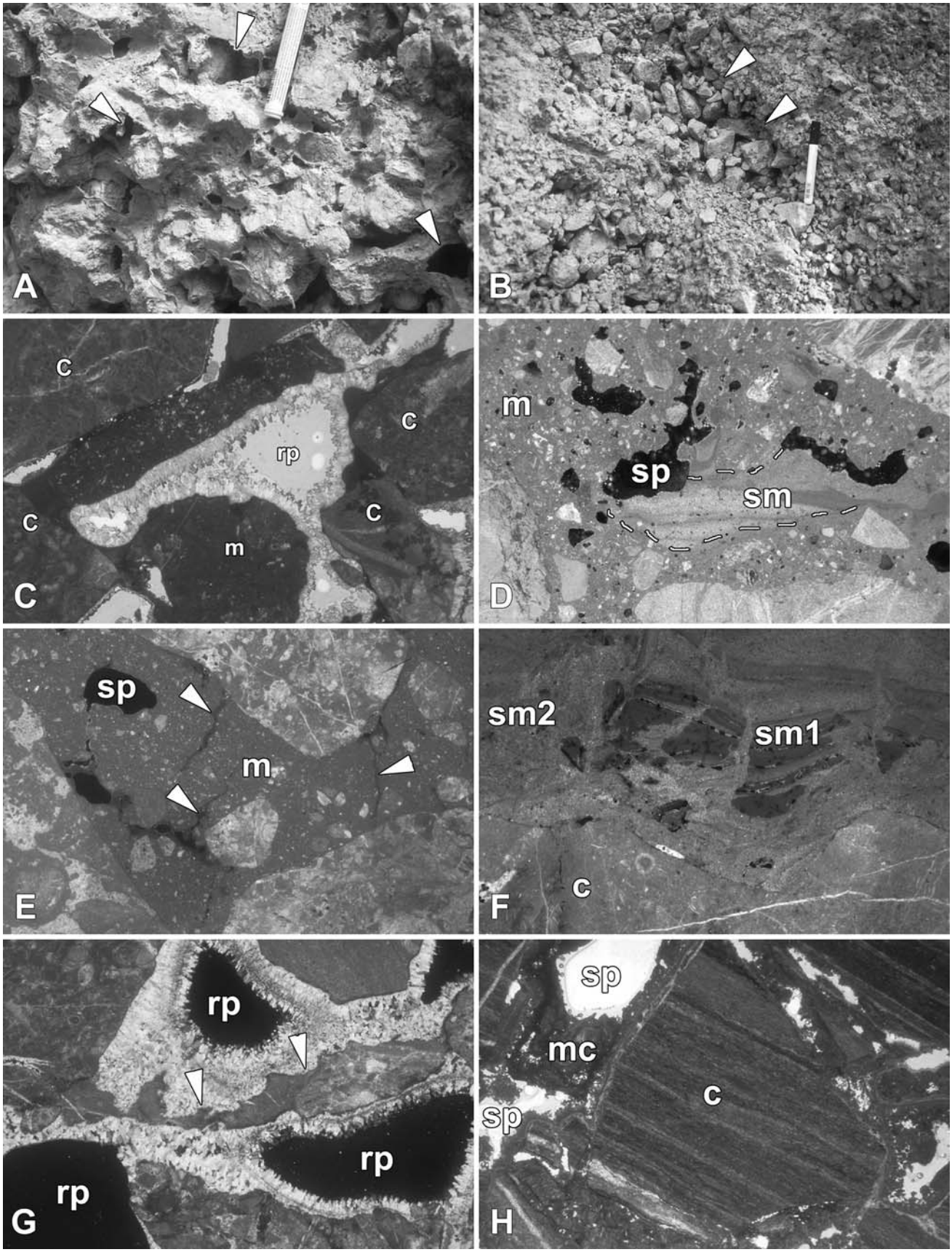
A
B
c
c
rp
c
c
c
m
C
m
sp
sm
D
sp
m
E
sm2
sm1
c
F
rp
rp
rp
G
sp
mc
c
sp
H

◀ **Fig. 7** Diagenetic features of lithified talus, Northern Calcareous Alps. **a** Open well pit in post-glacial talus slope. Cohesive debris flow deposit immediately above the openwork layer shown in Fig. 6**c**, about 4.5 m below the present surface. The matrix is riddled by a network of open veins up to about 2 cm in width (a few labelled by *arrowtips*). The vein lumen is fringed by a submillimeter-thin fringe of skalenohedral calcite cement; the fine-grained matrix is firm but friable. Sankt Veit, Mieming massif. *Pen tip* is 15 mm in width. **b** Open well pit in post-glacial talus slope. The talus here consists of cohesive debris flow breccias with a primary matrix of lime mud. In this deposit, discordant *cylindrical dykes* are present that show openwork fabric (*arrowtips*), and that are percolated by groundwater. Sankt Veit, Mieming massif. *Pen* is 14 cm in length. **c** Photomicrograph of cohesive debris flow breccia; lithoclasts labelled *c*. Primary matrix (*m*) of carbonate-lithic wackestone is riddled by large secondary pores coated by an isopachous fringe of skalenohedral calcite spar. Note remnant pore space (*rp*). Törl, Karwendel. Width of view 17 mm. **d** Photomicrograph of cohesive debris flow breccia, with a primary matrix (*m*) of lithic wackestone. In the matrix, a secondary pore (indicated by *dashed line*) had been filled by a secondary matrix (*sm*) of laminated lime mudstone. A subsequent phase of pore formation is recorded by open secondary pores (*black dots*, *sp*). Crossed nicols. Width of view 17 mm. **e** Photomicrograph of conglobreccia deposited from cohesive debris flow with a primary matrix (*m*) of lithic wackestone. The matrix is riddled by short, narrow cracks (a few labelled by *arrowtips*) that are subvertical to clast surfaces, and by secondary, open micro- to macropores (*black dots*, *sp*). Hohljoch-Ahornboden breccia, Karwendel. Crossed nicols. Width of view 17 mm. **f** Photomicrograph of talus breccia (lithoclast labelled *c*) that originally had an openwork clast fabric. A first generation of laminated secondary matrix (*sm1*) became fractured and partly dissolved. Matrix *sm1*, in turn, became embedded in another secondary matrix (*sm2*) of lime mudstone. Törl, Karwendel. Crossed nicols. Width of view 12 mm. **g** Photomicrograph of talus breccia. The breccia is lithified by an isopachous fringe of skalenohedral calcite cement, facing into open remnant pores (*rp*). Note pitted outline of lithoclasts (labelled by *arrowtips*), in contact to the calcite cement. Treffnerriegel, Gesäuse. Crossed nicols. Width of view 17 mm. **h** Photomicrograph of talus breccia composed of dolostone clasts (*c*), lithified by micritic to micropeloidal cement (*mc*). The cement, in turn, is riddled by secondary (*sp*). Schloßbach gorge, Freyungspitz massif. Width of view 17 mm

spar cements may originate from atmospheric CO_2 (−8.0‰) or from soil-derived CO_2 (typically −16 to −25‰; Lohmann 1988). Calcite formed in exchange with air–CO_2 tends towards an isotopic composition reflecting the air–CO_2. Conversely, calcite precipitated in open-system equilibrium with soil–gas CO_2 is limited to $\delta^{13}C$ values of about −15‰ (Rightmire and Hanshaw 1973). Together, for the sparitic cements, the evidence suggests an overriding air-derived $\delta^{13}C$ signal; contribution of soil CO_2 and host-rock buffering are subordinate in significance.

The $\delta^{18}O$ signature of meteoric cements is mainly influenced by temperature, geographic latitude (taken as 47°N for all samples), and altitude (Dansgaard 1964; Hoefs 1997; Hays and Grossman 1991). Palaeotemperature calculations based on the formula of Hays and Grossman (1991) yielded a temperature range from 3 to 33 °C. As compared with present mean annual temperatures (Fliri 1975), however, calculated values above 10–12°C are not realistic. In the eastern Alps, at present $\delta^{18}O$ decreases by −0.16‰ per 100 m increase in altitude (Humer et al. 1995). Our calculations with $\delta^{18}O$ of the sparitic cements resulted in an altitude effect of −0.11‰ per 100 m. This may broadly support that the isotope signature of the sparitic cements is largely determined by meteoric water.

Overall, however, a limited interpretability of $\delta^{13}C$ and $\delta^{18}O$ of the sparitic cements is obvious. As mentioned, dissolution of lime–muddy matrix and, locally, of diagenetically unstable lithoclasts were important sources for cementation. In addition, leaching of Würmian basal till that in many cases overlies talus relicts may also have contributed to lithification. All these sources may have led to rock buffering of the pore fluids, to an amount probably minor but difficult to quantify. Moreover, in mountain regions, the 'neutral depth' below which the temperature of groundwater is close to the medium-term (years to tens of years) mean temperature is some 15–50 m below the surface (Griebler and Mösslacher 2003). In talus slopes, the neutral depth probably is situated near the deeper end of this range. A large share of lithification thus may have proceeded under the influence of attenuated seasonal temperature changes, and under limited exchange with air–CO_2. Finally, the observation that deep, 'old' groundwaters may enter talus-slope successions from underneath further impedes interpretability of stable isotope values.

Diagenetic pathways in relation to facies architecture

Relative to the facies architecture of talus-slope successions, despite variations among the investigated talus relicts, a characteristic distribution of three basic diagenetic patterns is identified (Table 3, Fig. 10):

(1) In the apical to upper proximal portions of lithified talus slopes, openwork clast fabrics, for instance from gravelly grain flows, typically record a type 1.1 diagenetic pathway (a in Fig. 10). Conversely, layers of cohesive debris-flow breccias show a type 1.2 diagenetic pathway or a more complicated type 1.3 pathway (see Table 3).

(2) Farther down slope, in the lower-proximal part of talus slopes, diagenesis tends to be more differentiated. Here, openwork clast fabrics are characterized by a type 2 diagenetic pathway typically with well-developed fringes of calcite spar. In the most common type 2.1 pathway, a crust of micritic cement is overlain by a fringe of skalenohedral calcite spar (b in Fig. 10). Less commonly, secondary matrix was infilled before cement precipitation, or took place between discrete phases of precipitation (type 2.2 and 2.3 pathways in Table 3). Alternatively, matrix-bearing lithologies

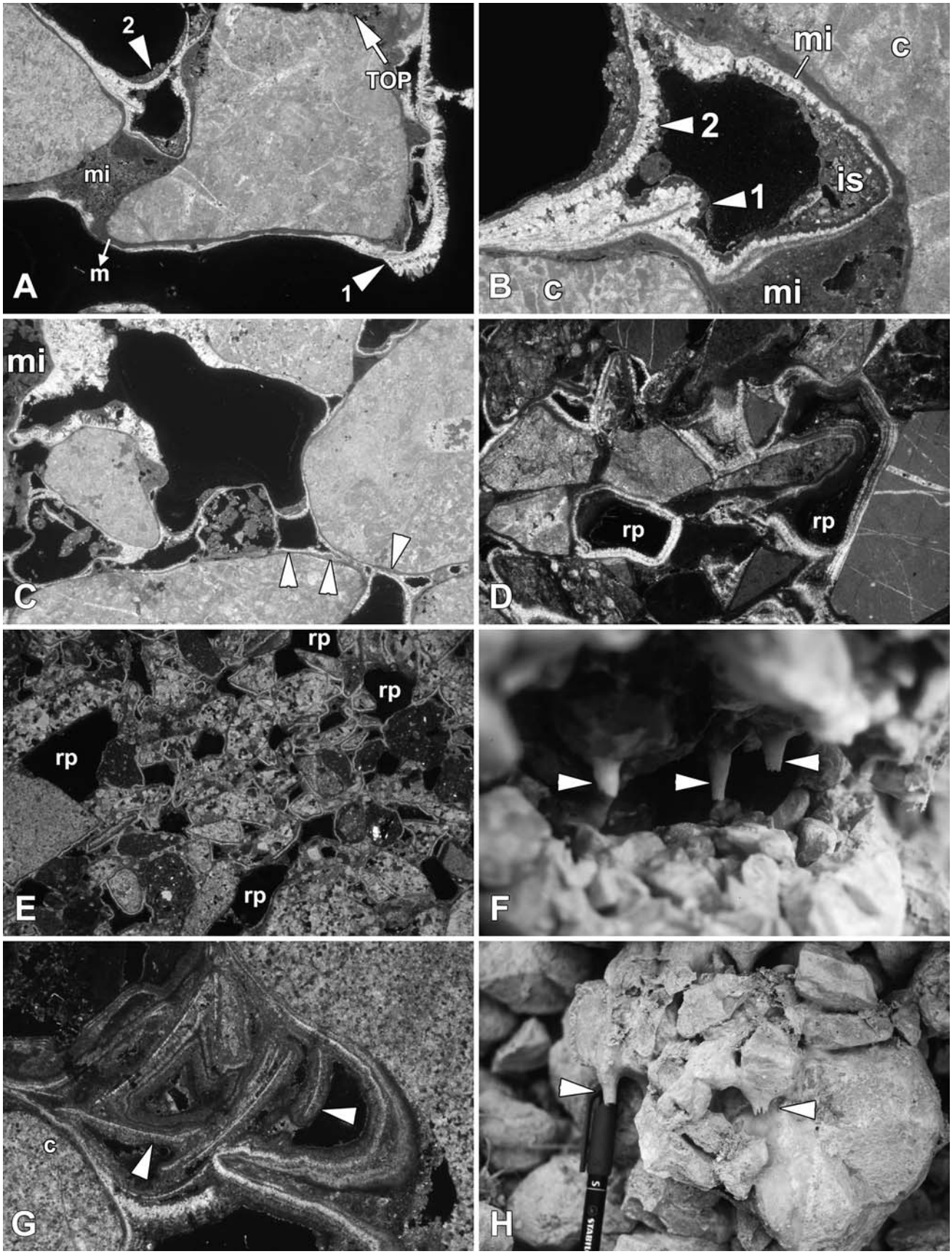
2
TOP
mi
m
A
1
mi
c
2
is
1
B
c
mi
mi
C
rp
rp
D
rp
rp
rp
rp
E
F
c
G
H

◀ **Fig. 8** Diagenetic features of lithified talus, Northern Calcareous Alps. **a** Photomicrograph of openwork conglobreccia, lithified by a crust of micritic cement (*m*), by patches of micropeloidal cement (*mi*), and by fringes of skalenohedral calcite spar. *Black* = *open pore space*. Note pendant cement (*arrowtip 1*), and the meniscus cement in the pore angle (*arrowtip 2*). Urschenbach, Karwendel. Crossed nicols. Width of view 17 mm. **b** Detail of preceding photo. Between clasts (*c*), the interstitial pore space is partly filled by micritic cement (*mi*), by fringes of calcite spar (*light-grey lines*), and by small patches of internal sediment (*is*) of lithic calcisiltite. Note incomplete preservation of meniscus cement labelled by *arrowtip 1*, and subsequent overgrowth by calcite spar. For spar fringe 2 (*arrowtip 2*), note that the main growth of cement is oriented inwards, towards the formerly water-filled meniscus. *Black* = *open pore space*. Crossed nicols. Width of view 5 mm. **c** Photomicrograph of openwork conglobreccia, lithified by crust of micritic cement (*very thin lines* labelled by *arrowtips*), by patches of micropeloidal cement (*mi*), and by different 'generations' of fringes of skalenohedral calcite cement (*light-grey lines*). Pore angles show meniscus cements. Urschenbach, Karwendel. *Black* = *open pore space*. Crossed nicols. Width of view 17 mm. **d** Photomicrograph of Holocene openwork talus breccia lithified by isopachous fringes of calcite cement (*light-grey lines*). Cementation of this talus deposit is associated with a limestone-precipitating spring. Straßberg gorge, Mieming massif (see Fig. 5). *Black* = *open remnant pores* (*rp*). Crossed nicols. Width of view 17 mm. **e** Photomicrograph of cemented apex of a talus slope that became partly lithified from an ephemeral water seepage out of the rock cliff immediately above. Breccia of angular clasts of dolostone, lithified by thin isopachous fringes of calcite cement (*thin light-grey lines* around clasts). *Black* = *open pore space* (*rp*). Rosengartl gorge, Imst. Crossed nicols. Width of view 10.5 mm. **f** Detail of same layer of openwork breccia as shown in Fig. 6**c**. Three small stalactites (labelled by *arrowtips*) pending from clast undersides. Width of view about 15 cm. **g** Photomicrograph of openwork talus breccia of clasts (*c*) of dolostones, and lithified by isopachous fringes of calcite cement. In larger interstitial pores, the cement fringes are arranged in stacked, geopetally oriented levels that represent former interstitial water levels (not meniscus cements). Collapsed platy cement fringes (*arrowtips*) may represent fragments of collapsed water-level cements and/or floe calcite formed on the interstitial water table. *Black* = *open pore space*. Schloßbach gorge, Freyungspitz massif. Crossed nicols. Width of view 11.5 mm. **h** Detail of openwork layer of conglobreccia. The interval is partly lithified by crusts of calcite cement and, locally, small stalactites (*arrowtips*). 990 m a.s.l., Urschenbach, Karwendel. *Pen tip* is 12 mm in width

(e.g., layers of cohesive debris flows) may record relatively complicated type 3 diagenetic pathways; the type 3 pathways result from repeated production of eluviation/dissolution pores, geopetal infilling of secondary matrices, and precipitation of micritic or sparitic cements (Table 3).

(3) In the distal part of talus successions, in cohesive debris-flow deposits, diagenesis is commonly associated with copious solution pores up to 10 cm in width, both after matrix and diagenetically unstable lithoclasts (c in Fig. 10). Lithomoulds may even be present in openwork clast fabrics. In the distal part of talus-slope successions, type 2 and type 3 diagenetic pathways tend to prevail. Conversely, in the few preserved thicker intervals of extremely poorly sorted rockfall breccias, type 1 diagenetic pathways were observed (d in Fig. 10).

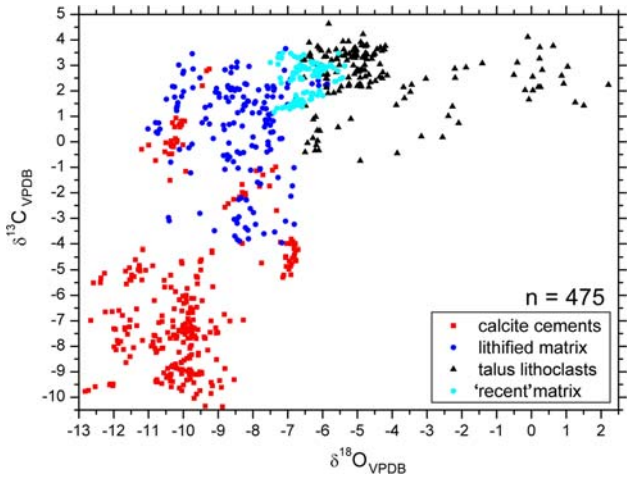

Fig. 9 Stable isotope values of oxygen and carbon of talus lithoclasts, matrices of carbonate mud, and of calcite spar cements. Note (a) that the isotope values of the fine-grained matrices are situated between talus gravels and sparitic cements, and (b) the roughly linear and co-variant trend towards more negative values of $\delta^{18}O$ and $\delta^{13}C$ from lithoclasts to cements. 'Recent' matrix refers to samples of fine-grained, carbonate-muddy matrix from active talus slopes. See text for Interpretation and Discussion

Interpretation

As a result of the position of a talus slope relative to the groundwater table, diagenesis may be driven by different relative amounts of site-derived meteoric pore water and deeper groundwaters. Downslope along well-preserved talus successions, the overall increase in the complexity of diagenetic pathways and the overall increase in sparitic cements (Fig. 10) reflects a prolonged presence of pore waters within the slope succession. In post-glacial, partly lithified talus slopes, precipitation of sparitic cement may proceed within a few tens of meters to a few meters below the surface. This suggests that, in those cases, cementation can be driven by local-derived meteoric waters. For a lithified talus succession that extends down to 1,000–1,200 m a.s.l, however, percolation of deep groundwater into the slope succession is established by hydrogeological investigations (cf. Heissel 1993).

The widespread type 2 diagenetic pathway from micritic cement to an isopachous fringe of calcite spar probably reflects progressive burial from a near-surface, vadose diagenetic setting to an essentially phreatic setting deeper within the talus succession. Alternatively, the change from micritic to sparitic cement might record a switch from an overall drier to a wetter climate. Because of a widespread presence of the type 2 diagenetic pathway, however, we

Table 3 Typical diagenetic pathways in relation to sedimentary facies (cf. Table 1, Fig. 10). Diagenetic products may be separated from each other by a phase of dissolution

Type 1 pathway. Typical for (a) openwork breccias to conglomerates, and (b) breccias and conglobreccias of cohesive debris flows
1.1: Micrite cement → infill of secondary matrix
1.2: Dissolution–reprecipitation of matrix → lithified matrix with dissolution porosity
1.3: Dissolution–reprecipitation of matrix → lithified matrix → dissolution porosity → infill of secondary or tertiary matrix → dissolution–reprecipitation → lithified later-stage matrix (potential open remnant pore space or later-stage dissolution porosity)
Type 2 pathway. Typical for openwork deposits such as (a) grain flow breccias, and (b) alluvial openwork breccias to conglobreccias. Aside of sparitic cement fringes around clasts, meniscus cements may also be present
2.1: Micrite cement → fringe of sparitic cement
2.2: Infill of secondary matrix → micrite cement → fringe of sparitic cement
2.3: Micrite cement → secondary matrix → fringe of sparitic cement
Type 3 pathway. May form in all deposits with or without primary matrix, in areas of prolonged or repeated pore-water supply. Diagenetic phases and products may interchange in arbitrary order, and all may be separated from each other by an intermittent phase of dissolution. Not all of the diagenetic products indicated below may be realized
Eluviation/dissolution of primary matrix (if present)
↓↑
Infill of secondary matrix
↓↑
Micritic cement
↓↑
Sparitic cement (fringes, menisci, water-level cements)

infer that the burial-related development was at least the more common one.

The type 3 diagenetic pathway is related to fluctuations in saturation state of pore waters for calcium carbonate. We infer that type 3 pathways are most common in the distal part of talus-slope successions because of overall higher availability/prolonged presence of pore waters. We could not identify a correlation between the age of a talus succession and diagenetic complexity.

Origins of carbonate-muddy matrix

The gravelly to cobbly, unstable surface layer of active talus slopes belies a significant content in carbonate mud down from about 20–50 cm within the slope. We had sampled the bulk sediment of the topmost meter of the apex of three selected rockfall-dominated talus slopes (two in limestone terrains, one in a dolostone terrain). In the apex of these talus slopes, 4–11% by weight of carbonate-muddy matrix with a grain size smaller than 0.063 mm is present (Fig. 11). Winter-snow relicts directly below the selected cliffs were coated by a layer up to about 1 cm in thickness of carbonate mud. The mineralogy of this mud, tested by XRD, is identical to that of the matrices sampled from adjacent talus slopes.

Inspection of matrices under SEM shows that they consist of grains down to less than a micron in size, but commonly the size range is gradual from 1–100 µm. Most grains larger than about 20–50 µm in size show a non-rhombohedral, irregular shape and dissolution channels. For the dolo-lithic talus slope, XRD of the matrix indicates only dolomite, that is, no calcite has newly formed; under SEM, the dolomitic grains are of irregular shape and show dissolution pits (Fig. 12a, b). In talus slopes composed of limestone clasts, a large proportion of grains is similarly of irregular shape and shows dissolution pits (Fig. 12c). With decreasing grain size down to about 1 µm, however, an increasing proportion of well-defined calcite rhombohedra is present (Fig. 12c, d). Stable isotope analyses of oxygen and carbon of unlithified matrices of active talus slopes show a shift is isotopic composition relative to the lithoclasts (Fig. 9).

Thin sections of ‘tintenstriche’ (=technical term for blackish ‘stripes’ of water seepage down rock cliffs that are colonized by cyanobacteria and lichens; Pentecost and Whitton 2000) in the rock cliffs above the sampled talus slopes show that the tintenstriche consist of a layer up to a few millimeters thick of friable micrite with interspersed coccoid cyanobacteria (e.g., *Gloeocapsa*, *Gloeothece*). In addition, both within and offside the tintenstriche, lichens calcify as stromatolites (Fig. 12e, f).

Interpretation

Three lines of evidence indicate that a significant part of the matrix in talus slopes is derived from the rock cliffs (Fig. 13). First, in the topmost meter of the apex of rockfall-dominated

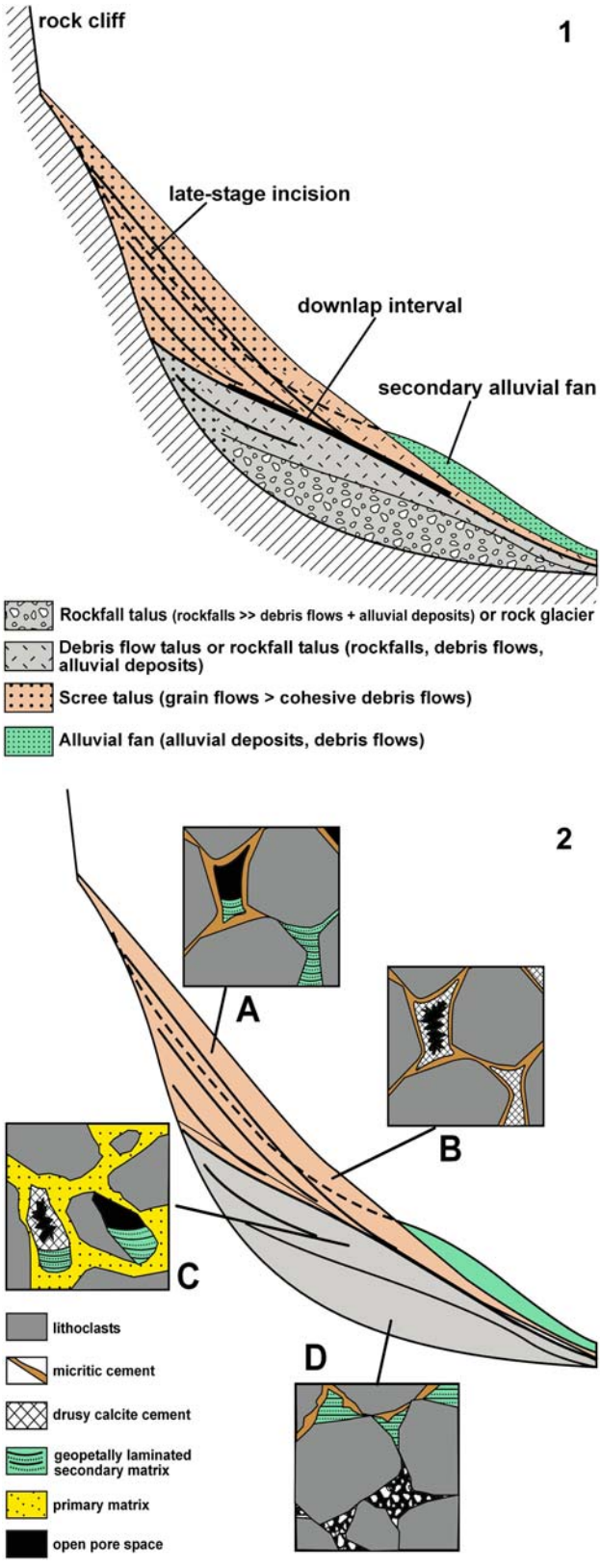

◀ **Fig. 10** Scheme of typical diagenetic features of lithified talus successions in relation to facies architecture. **1** Generalized facies architecture of mature talus slope succession. **2** Diagenetic products. *A* In the apical to upper-proximal part of talus slopes, lithification is mainly by micritic cements and/or by lithification of secondary matrices; fringes of spar cement are subordinate in abundance. *B* In the lower-proximal part of talus slopes, lithification is mainly by crusts of micritic cement overlain by calcite spar. *C* In the (stratigraphically) lower and distal part of talus successions, in deposits of lime-muddy cohesive debris flows, diagenesis is characterized by lithification of lime-muddy matrix, by dissolution attack of mineralogically unstable lithoclasts, by infilling of secondary matrices, and by isopachous fringes to pore-filling calcite spar cements. *D* In the stratigraphically basal part of successions, in rockfall deposits, lithification is mainly by crusts of micritic cements, and/or by lithification of secondary matrices, and/or by precipitation of thin crusts of micritic cements in an interstitial 'rubble' of carbonate-lithic sand to silt. In the medial to distal part of talus successions, multi-phase diagenetic pathways (type 3 pathways, see Table 3) more complicated but with a similar inventory of processes and products than those indicated in figure are locally present

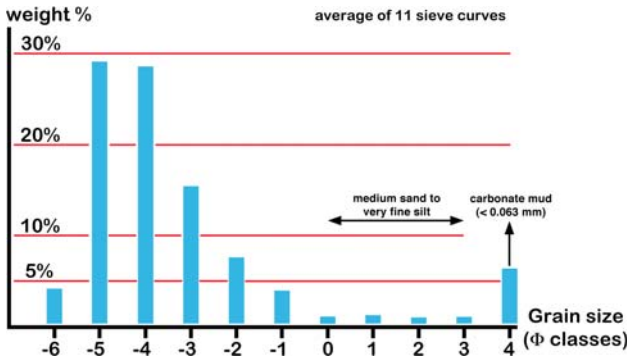

Fig. 11 Grain-size distribution in the apex (nine values) and in the upper-proximal part (two values) of rockfall-dominated talus slopes. Note paucity in medium sand to very fine silt, and the distinct content in carbonate mud (6.5 wt% average, 4–11 wt% range)

talus slopes, fine-grained matrix can hardly result from prolonged clast abrasion. Second, the biogenic calcification adjacent to and mainly within the tintenstriche indicates that carbonate rock cliffs in part degrade by being turned to microbially induced micrite. Third, the presence of mineralogically identical carbonate mud on snow relicts at the toe of the same cliffs underscores a derivation of the mud from the cliff. Colonization of cliff surfaces by endolithic microbial assemblages weakens and micritizes the rock surface (Hoppert et al. 2004); the weakened rock surface is susceptible to attrition by stone-laden rain wash and snow shear. Along the tintenstriche, groundwater seeping from rock joints becomes evaporative concentrated, until precipitation of micrite is induced or aided by the photosynthesis of the rock-coating biotic community (Fig. 13) (Kilian 2008; cf. Pentecost and Whitton 2000). The calcified lichens and cyanomats on the cliffs are quite thin (Fig. 12e). A single event of removal of the biomats, as well as abrasion of a micritized rock surface, yields only a minute amount of micrite. Lithobiontic organisms on carbonate rocks, however, are effective epi- and endo-lithic colonizers (Hoppert et al. 2004). Persistent growth and calcification of

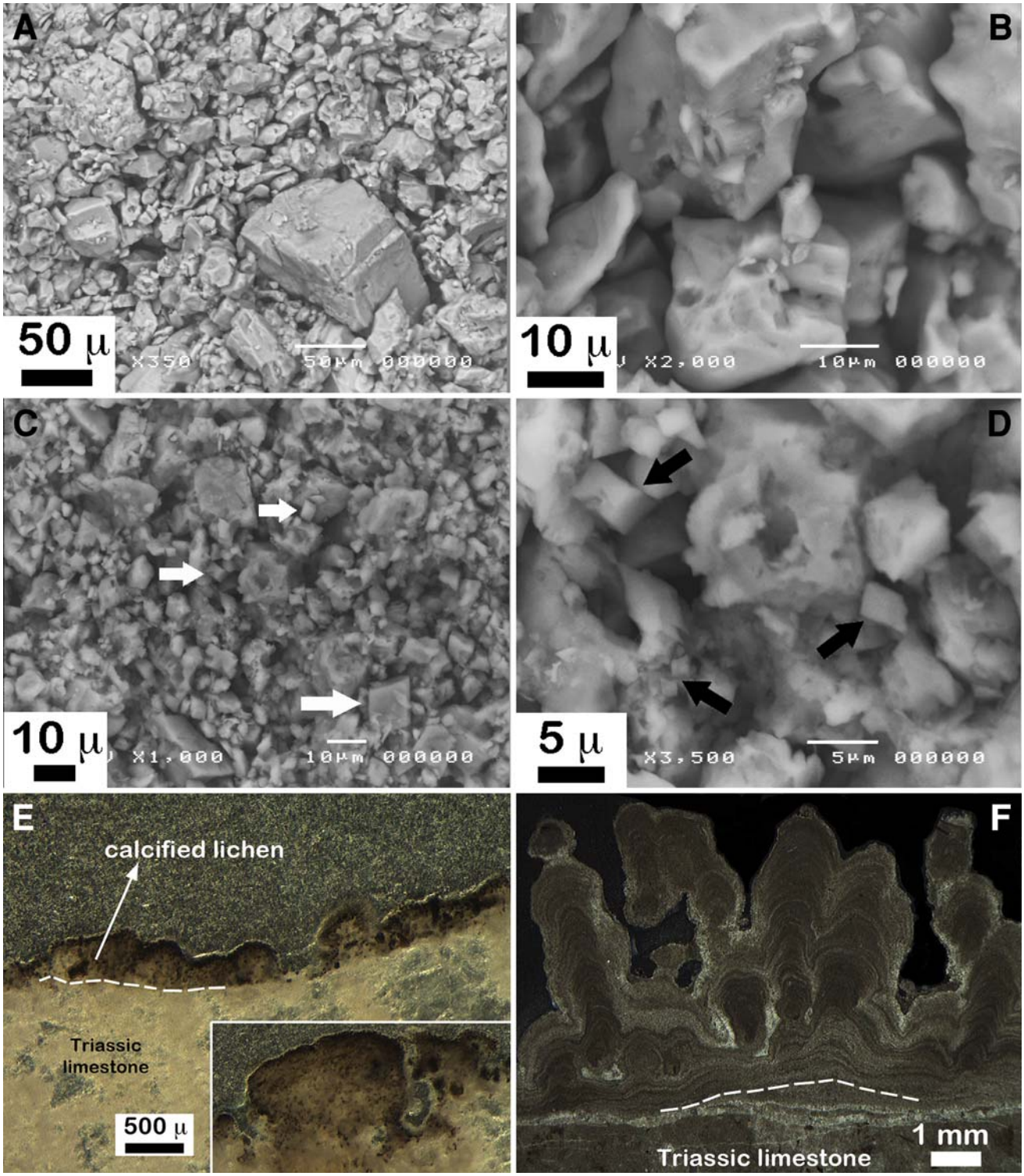

Fig. 12 Matrices of active rockfall-dominated talus slopes, and calcified biomats of rock cliffs. **a** SEM image of dololithic matrix. Except for the large grain near center, note absence of plane crystal surfaces. **b** Detail of preceding photo. The matrix consists of grains of highly irregular, pitted and embayed shape. **c** SEM image of calcilithic matrix. In this matrix, many grains are of highly irregular, pitted shape but many others are well-defined rhombohedra of calcite (a few labelled by *white arrows*). **d** Detail of preceding photo. Among calcite grains of irregularly pitted shape, well-defined rhombohedral crystals of calcite are present (*black arrows*). **e** Micritic lichen thrombolite (probably of *Verrucaria nigrescens*) from a tintenstrich in a cliff above a rockfall-dominated talus slope. The *tiny black specks* are coccoid cyanobacteria. Crossed nicols, dark-field microscopy. *Scale bar* holds also for inset. **f** Micritic, digitate lichen stromatolite produced by *Pertusaria corallina* in a cliff above a rockfall-dominated talus slope. Note the thickness of the stromatolithic layer. Crossed nicols

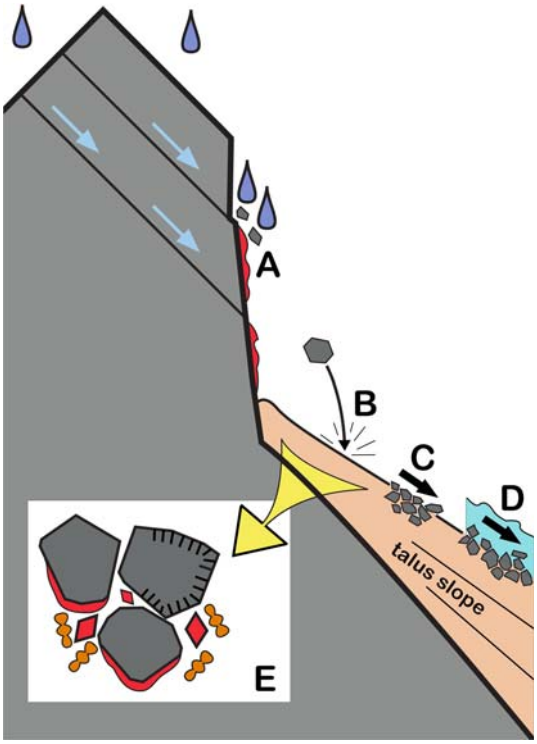

Fig. 13 Provenance of carbonate-muddy matrix in talus slopes. Along water seepages out of cliffs, calcified tintenstriche (shown *red*) produced by lichens and/or cyanobacteria form (*A*). Upon abrasion of the cliff, for instance, by stone-laden rain wash, or by snow cascading down, the micrite of the tintenstriche is transported to the apical part of the talus slope. In addition, abrasion of microbored cliff surfaces results in physical production of micrite. Impact of rockfalls (*B*), abrasion of talus clasts in grain flows (*C*), and abrasion of clasts along the base of, both, slowly downslope-moving snow sheets and snow avalanches (*D*) probably also are sources of fine-grained matrix. Within the talus slope, production of micrite by repeated cycles of dissolution and evaporation, and from microbial mediation, may represent another source of carbonate mud (*E*). Upon vadose dissolution followed by re-precipitation as cement in deeper levels within the talus-slope succession, the early-produced carbonate mud in talus slopes may support a large part of lithification

biomats, and the persistent microboring by eu-endolithic communities, in permanent competition with abrasion and frost spalling, thus may ultimately result in a large amount of micrite.

The matrices of talus slopes may be of different diagenetic reactivity. For the dolo-lithic matrix, its composition of irregular crystal fragments with pitted, embayed surfaces suggests that this matrix is subject to dissolution only. Conversely, the well-defined calcite rhombohedra in the matrix of talus slopes composed of limestone clasts may represent newly formed calcimicrite. Early diagenetic changes in the unlithified matrix of active talus slopes are supported by the shift in stable isotope values of oxygen and carbon between matrix and lithoclasts.

Farther down along talus slopes, however, a contribution of matrix from clast abrasion upon talus shift is probable. ‘Talus shift’, that is, a slow net downslope movement of all clasts, for instance is caused by grain flows, snow drag, passing deer or man, and rockfall impact (Fig. 13). Dissolution of clast surfaces followed by biologically supported reprecipitation as micrite may represent another source of micritic matrix. Furthermore, freeze-thaw cycles may not only lead to production of talus clasts, but may also favor precipitation of micrite.

Discussion

As mentioned, lithified talus relicts are by far the most common in the NCA. Although the thick metadolostone successions of the Central-Alpine Mesozoic (CAM) (Fig. 1) weather under copious production of dolo-lithic matrix, no lithification takes place. It may be related to both the abundance in cohesive mud, promoting surface runoff, and to the dolomite mineralogy of the matrix that the talus slopes of the CAM remain unlithified. The common presence of lithified talus relicts in the NCA thus primarily results from their lithological composition (Fig. 2).

Much of the calcium required for lithification may stem from dissolution of micritic matrix and/or of lithoclasts, that is, from within the talus succession itself (Table 4). This is indicated by the partly lithified, post-glacial talus successions not veneered by glacial till. Cementation may also be supplied, in part at least, from ‘external’ sources, such as: (a) leaching of overlying glacial till, (b) percolation of deep groundwater into the talus slope, or (c) emergence of a limestone-precipitating spring closely above the talus (Fig. 4; Table 4). For the Eastern Alps, a strong positive correlation between areas of glacial till with presence of limestone springs suggests that till contributes to dissolved calcium carbonate in meteoric groundwaters (Sanders et al. 2006a, 2006b). Leaching experiments with lodgement till underscore that it may be an effective source of dissolved calcium carbonate (Rüf 2006). Furthermore, a correlation between lithification of interglacial deposits and presence of overlying glacial till is identified for many Quaternary successions in northern Germany (Elbracht 2002). Seepage of deep/longer-travelled groundwater into a talus succession already lithified has been documented in one case (see above). Entrance of deep groundwaters into talus slopes may be relatively common, but is difficult to test. Indeed, the few limestone-precipitating springs shedding onto talus slopes may be seen as a mirror image to groundwaters entering from underneath into a talus succession.

The most notable observation with respect to both the sedimentology and diagenesis of talus-slope successions is their richness is carbonate mud. Depending on sorting, the

Table 4 Sources of calcium carbonate for cementation of talus successions

Source of $CaCO_3$	Process	Remarks
Internal sources (=sources from talus succession itself)	Dissolution of lime–muddy matrices	Widespread, significant source
	Dissolution of lithoclasts	Common, locally a significant source
External sources (=sources situated outside the talus succession)	Micrite production in rock cliff above talus	Widespread, significant source
	Leaching of glacial till overlying the talus succession	Probably common, locally significant
	Entrance of percolating deep groundwater into talus slope	Probably significant
	Emergence of limestone-depositing spring upslope the talus succession	Uncommon but effective
	Aeolian input of fine-grained carbonate-lithic material	Significance not yet established; questionable

interstitial pore space of clast-supported talus breccias ranges between 35 and 50%. Irrespective whether a talus slope is dominated by deposits of cohesive debris flows or of openwork grain flows, a substantial proportion of total volume is carbonate mud as primary and secondary matrices. Aside of karstic dissolution and production of coarse rock fragments, thus, carbonate-rocky terrains such as the NCA initially also degrade under significant formation of carbonate mud. A quantitative estimate of the relative proportions of, each karstic dissolution, coarse rock fragments, and mud is hardly possible as yet. Further investigations are required to better unravel the workings of the hitherto unrecognized 'montane carbonate mud factory'.

Conclusions

1. In the Northern Calcareous Alps (NCA), lithified and partly lithified carbonate-rocky talus slopes are common. Talus lithification proceeded mainly by precipitation of micritic cements and of sparitic calcite cements, and by micron-scale dissolution–reprecipitation in lime–muddy matrices.
2. Precipitation of vadose and phreatic cements was nourished (a) internally, by dissolution of lime–muddy matrices and of lithoclasts of a talus slope, and/or (b) externally, by leaching of glacial till, by groundwater entrance from underneath or, more rarely, by emergence of limestone-precipitating spring above a talus slope.
3. In the steep-dipping (35–30°), proximal part of talus-slope successions, comparatively simple diagenetic pathways including micritic cement, (skalenohedral) calcite spar, and geopetally infilled secondary matrices of lime mudstone are typical. In the low-dipping (20–5°), distal part of talus slopes, more complicated diagenetic pathways are common. The overall downslope gradient in diagenetic pathways is interpreted as a result of prolonged availability of pore waters from the apex to the toe of slope.
4. Cementation of different talus relicts, determined by $^{234}U/^{230}Th$ dating of sparitic cements, took place during different times, over a total documented age range of 5–480 ka. Cement precipitation can start and proceed within a few hundreds to a few thousands of years after accumulation of a talus slope. Depending on hydrologic regime, however, later diagenetic changes may take place.
5. Carbonate-rocky talus slope successions contain a significant amount of carbonate mud. The mud probably results from combined effects of (a) abrasion, (b) physical weathering, and (c) by carbonate dissolution followed by reprecipitation as micrite either on the cliff surface and/or within the vadose zone of talus slopes. Upon early geomorphic degradation, thus, a portion yet hardly quantified of the NCA is converted to mud-sized carbonate sediment.

Acknowledgements Financial support from project 16114-NO6 'Quaternary talus, Northern Calcareous Alps' of the Austrian Research Foundation (to D.S.), and from project 'Kalktuff in Vorarlberg' funded by inatura Erlebnisschau Dornbirn (to D.S.) is gratefully acknowledged. Discussions with Christoph Spötl and Karl Krainer, Institute of Geology and Palaeontology, University of Innsbruck, and field trips with Alfred Gruber, Geological Survey of Austria (Vienna) and Christoph Prager, alpS Center for Natural Hazard Management, Innsbruck, are acknowledged. Franz Riepler of enterprise 'GWU Geologie-Wasser-Umwelt', Salzburg, is thanked for an important hint on a man-made well pit into talus. The paper gained from the reviews of Leslie Melim, Western Illinois University (USA), and André Freiwald, University of Erlangen (Germany).

References

Ampferer O (1907) Über Gehängebreccien der nördlichen Kalkalpen. Jahrbuch geol Reichsanst 57:727–752

Ampferer O (1914) Über die Aufschliessung der Liegendmoräne unter der Höttinger Brekzie im östl Weiherburggraben bei Innsbruck. Zeitschrift f Gletscherkunde 8:145–159

Ampferer O (1935) Geologischer Führer für die Gesäuseberge. Geologische Bundesanstalt, Vienna, 177 pp

Bates RL, Jackson JA (eds) (1980) Glossary of geology. American Geological Institute, Falls Church (Va), 749 pp

Bathurst RC (1975) Carbonate sediments and their diagenesis. In: Developments in sedimentology, vol 12. Elsevier, Amsterdam, 658 pp

Bertran P, Texier J-P (1994) Structures sédimentaires d'un cone de flots de débris (Vars, Alpes francaises méridionales). Permafr Periglac Proc 5:155–170

Dansgaard W (1964) Stable isotopes in precipitation. Tellus 16:436–468

Debaene G (2003) Uranium-series dating of marly sediments: applications to Jaroszów fossil lake (SW Poland). Geochronometria 22:15–26

Elbracht J (2002) Karbonatische Zementation pleistozäner Lockersedimente NW-Deutschlands, Unpublished Ph.D. thesis, University of Hannover, 214 pp

Fliri F (1975) Das Klima der Alpen im Raume von Tirol. Universitätsverlag Wagner, Monographien zur Landeskunde Tirols, Innsbruck-München, 454 pp

Flügel E (2004) Microfacies of carbonate rocks. Springer, Heidelberg, 976 pp

Frank N, Braum M, Hambach U, Mangini A, Wagner G (2000) Warm period growth of travertine during the last interglaciation in southern Germany. Quat Res 54:38–48

Geyh MA (2001) Reflections on the $^{230}Th/^{234}U$ dating of dirty material. Geochronometria 20:9–14

Geyh MA (2005) Handbuch der physikalischen und chemischen Altersbestimmung. Wissenschaftliche Buchgesellschaft, Darmstadt, 211 pp

Griebler C, Mösslacher F (2003) Grundwasser-Ökologie. Facultas, Vienna, 495 pp

Hays PD, Grossman EL (1991) Oxygen isotopes in meteoric calcite cements as indicators of continental paleoclimate. Geology 19:441–444

Heissel G (1993) Die Hydrogeologie der Mühlauer Quellen im Lichte geologischer und strukturgeologischer Erkenntnisse unter Einbeziehung besonderer Aspekte der Geologie Tirols. Landesgeologie Tirol 1:1-43. Amt der Tiroler Landesregierung, Athesia Tyrolia Druck, Innsbruck

Hoefs J (1997) Stable isotope geochemistry. Springer, Heidelberg, 201 pp

Hoppert M, Flies C, Pohl W, Günzl B, Schneider J (2004) Colonization strategies of lithobiontic microorganisms on carbonate rocks. Environ Geol 46:421–428

Humer G et al (1995) Niederschlagsisotopennetz Österreich. Monographien UBA 52:86

Kaufman A (1993) An evaluation of several methods for determining $^{230}Th/^{234}U$ ages in impure carbonates. Geochim Cosmochim Acta 57:2303–2317

Kaufman A, Broecker WS (1965) Comparison of ^{230}Th and ^{14}C ages for carbonate materials from lakes Lahontan and Bonneville. J Geophys Res 70:4039–4054

Kilian S (2008) Untersuchung der feinkörnigen Matrix in aktiven, felssturz-dominierten Talus-Hängen. Unpublished BSc Thesis, University of Innsbruck, 44 pp

Ladurner J (1956) Mineralführung und Korngrössen von Sanden (Höttinger Breccie und Umgebung). Tschermaks mineral petrogr Mitt 5:102–109

Lin JC, Broecker WS, Anderson RF, Hemming S, Rubenstone JL, Bonani G (1996) New $^{230}Th/^{234}U$ and ^{14}C ages from Lake Lahontan carbonates, Nevada, USA, and a discussion of the origin of initial thorium. Geochim Cosmochim Acta 60:2817–2832

Lohmann KC (1988) Geochemical patterns of meteoric diagenetic systems and their application to studies of paleokarst. In: James NP, Choquette PW (eds) Paleokarst. Springer, Heidelberg, pp 58–80

Ludwig KR, Titterington DM (1994) Calculation of $^{230}Th/^{234}U$ isochrons, ages, and errors. Geochim Cosmochim Acta 58:5031–5042

Mallick R, Frank N (2002) A new technique for precise uranium-series dating of travertine micro-samples. Geochim Cosmochim Acta 66:4261–4272

Obojes U (2003) Quartärgeologische Untersuchungen an den Hängen der Innsbrucker Nordkette (Höttinger Breccie). Unpubl Diploma Thesis, Univ of Innsbruck, 89 pp

Ostermann M (2006) Thorium–uranium age-dating of "impure" carbonate cements of selected Quaternary depositional systems of western Austria: results, implications, problems. Unpublished PhD Thesis, University of Innsbruck, 173 pp

Ostermann M, Sanders D, Kramers J (2006a) $^{230}Th/^{234}U$ ages of calcite cements of the proglacial valley fills of Gamperdona and Bürs (Riss ice age, Vorarlberg, Austria): geological implications. Austrian J Earth Sci 99:31–41

Ostermann M, Sanders D, Kramers J (2006b) Uranium/thorium age-dating of "impure" carbonate cements of selected Quaternary depositional systems of western Austria: results and implications. In: Pangeo Austria 2006. Innsbruck Univ Press Conf Series, Innsbruck, pp 233–234

Ostermann M, Sanders D, Prager C, Kramers J (2007) Aragonite and calcite cementation in 'boulder-controlled' meteoric environments on the Fern Pass rockslide (Austria): implications for radiometric age-dating of catastrophic mass movements. Facies 53:189–208

Patzelt G (1980) Neue Ergebnisse der Spät- und Postglazialforschung in Tirol. Jahresber d Österr Geogr Ges 76/77:11–18

Pentecost A, Whitton BA (2000) Limestones. In: Whitton BA, Potts M (eds) The ecology of cyanobacteria. Kluwer, Dordrecht, pp 257–279

Rightmire CT, Hanshaw BB (1973) Relationship between carbon isotope composition of soil CO_2 and dissolved carbonate species in groundwater. Water Resour Res 9:958–967

Rosholt N (1976) $^{230}Th/^{234}U$ dating of travertines and caliche rinds (abstr.). Geol Soc Am Abstr Progr 8:1079

Rüf B (2006) Quelltuff in Vorarlberg—Sedimentologische, materialkundliche und bauhistorische Aspekte. Unpublished Diploma Thesis, University of Innsbruck, 173 pp

Sanders D, Ostermann M (2006) Depositional setting of the sedimentary rocks containing the "warm-interglacial" fossil flora of the Höttinger Brekzie (Pleistocene, Northern Calcareous Alps, Austria): a reconstruction. Veröff Tiroler Landesmus Ferdinandeum 86:91–118

Sanders D, Wertl W (2009) 'Cool-spring' carbonate deposystems, Eastern Alps: controls on formation and mineralogy (abstr.). Geophys Res Abstr 11:EGU2009-2730

Sanders D, Unterwurzacher M, Rüf B (2006a) Microbially induced calcium carbonate in tufas of the western Eastern Alps: a first overview. Geo Alp 3:167–189

Sanders D, Krainer K, Unterwurzacher M (2006b) Geological controls on formation of tufa-precipitating spring (Eastern Alps): what do the maps tell? In: Pangeo Austria 2006. Innsbruck Univ Press Conf Series, Innsbruck, pp 291–292

Sanders D, Prager C, Ostermann M, Kramers J, Haas U (2007) Local cementation of carbonate-lithic rockslides: prerequisite to $^{234}U/^{230}Th$ proxy-dating the mass-wasting event (abstr.). Geo Alp 4:32

Sanders D, Tessadri R, Rott E (2008) Quaternary spring-associated limestones of the Eastern Alps: implications for marine carbonates (abstr.). Geophys Res Abstr 10:EGU2008-A-02104

Sanders D, Ostermann M, Kramers J (2009) Quaternary carbonate-rocky talus slope successions (Eastern Alps, Austria): sedimentary facies and facies architecture. Facies (in press). doi: 10.1007/s10347-008-0175-z

Schmid SM, Fügenschuh B, Kissling E, Schuster R (2004) Tectonic map and overall architecture of the Alpine orogen. Eclogae geol Helvetiae 97:93–117

Schrott L, Hufschmidt G, Hankammer M, Hoffmann T, Dikau R (2004) Spatial distribution of sediment storage types and quantification of valley fill deposits in an alpine basin, Reintal, Bavarian Alps, Germany. Geomorphology 55:45–63

Spötl C, Vennemann T (2003) Continuous-flow isotope ratio mass spectrometric analysis of carbonate minerals. Rapid Commun Mass Spectrom 17:1004–1006

Van Husen D (1999) Geological processes during the Quaternary. Mitt österr geol Ges 92:135–156

Van Vliet-Lanoe B (1976) Traces de ségrégation de glace en lentilles associées aux sols et phénomènes périglaciaires fossiles. Biuletyn Periglacjalny 26:41–55

Darling WG, Bath AH, Gibson JJ, Rozanski K (2005) Isotopes in water. In: Leng MJ (ed) Isotopes in palaeoenvironmental research. Dev Palaeoenviron Res, vol 10, pp 1–66